


Facile preparation of Co₃O₄ nanoparticles incorporating with highly conductive MXene nanosheets as high-performance anodes for lithium-ion batteries

 The corrections made in this section will be reviewed and approved by a journal production editor.

Yinchao **Zhao** Writing - review & editing Writing - original draft Investigation Methodology Conceptualization ^{a,b}, Chenguang **Liu** Writing - review & editing Methodology Conceptualization ^{a,b}, Ruowei **Yi** Writing - review & editing Conceptualization ^{c,d}, Ziqian **Li** Investigation Methodology ^a, Yanbing **Chen** Investigation Methodology ^a, Yinqing **Li** Resources ^e, Ivona **Mitrovic** Supervision ^b, Stephen **Taylor** Supervision ^b, Paul **Chalker** Supervision ^f, Li **Yang** Funding acquisition Supervision Writing - review & editing Writing - original draft Resources ^{d,**} li.yang@xjtlu.edu.cn, Cezhou **Zhao** Funding acquisition Supervision Resources ^{a,*} cezhou.zhao@xjtlu.edu.cn

^aDepartment of Electrical and Electronic Engineering, Xi'an Jiaotong-Liverpool University, Suzhou, 215123, China

^bDepartment of Electrical Engineering and Electronics, University of Liverpool, Liverpool, L69 3GJ, United Kingdom

^cStephenson Institute for Renewable Energy, Department of Chemistry, University of Liverpool, Liverpool, L69 7ZD, United Kingdom

^dDepartment of Chemistry, Xi'an Jiaotong-Liverpool University, Suzhou, Jiangsu, 215123, China

^eDongguan Hongde Battery Ltd.Co., Dongguan, 523649, China

^fCentre for Advanced Materials, University of Liverpool, L69 3GH, United Kingdom

*Corresponding author.

**Corresponding author.

Abstract

There is considerable scientific interest in the newly available family of MXenes material. An analog as graphene, this two-dimensional (2D) layered material with the structure of transition metal carbides or nitrides exhibits superior electronic conductivity, large interlayer spacing for highly efficient lithium ions diffusion pathways and environmental benignity, making it useful as energy storage material. However, the inferior capability to store lithium ions impedes its wide application in lithium-ion batteries. Therefore, a facile strategy for preparing Co_3O_4 nanoparticles incorporated with MXene nanosheets on Ni foams has been developed. Small-size Co_3O_4 nanoparticles are uniformly distributed within the MXene nanosheets leading to **the** highly efficient lithium ions and electrons transmission, as well as the prevention for the restacking of MXene nanosheets and huge volume change of the Co_3O_4 nanoparticles. Under the cooperative effect of Co_3O_4 nanoparticles and MXene nanosheets, the $\text{Co}_3\text{O}_4/\text{MXene}$ composite electrode with the mass ratio of $\text{Co}_3\text{O}_4/\text{MXene} = 1:1$ exhibits an excellent reversible capacity of 1005 mAh g^{-1} after 300 cycles at the current density of 1 C, which significantly exceeds that of pristine Co_3O_4 electrode. Though the current density climbs to 5 C, the composite electrode remains a stable capacity of 307 mAh g^{-1} after 1000 cycles. It is demonstrated that $\text{Co}_3\text{O}_4/\text{MXene}$ composite electrode has the potential as an anode for the high-performance lithium-ion batteries.

Keywords: Binder-free; Co_3O_4 ; Lithium-ion batteries; MXene

1 Introduction

Lithium-ion batteries (LIBs) have been regarded as one of the most promising candidates for non-recyclable fossil-fuel resources that cause long-term and devastating pollution to the environment. Nevertheless, the commercial graphite-based LIBs possessing a low theoretical capacity (372 mAh g^{-1}) is no longer to fulfill the upsurging demand for energy resources and storage technologies. Hence, many progressive researchers **have** devoted to developing LIBs with high energy density and cycling stability. In this regard, transition metal oxides (TMOs: CuO , NiO , Fe_3O_4 , TiO_2 , and Co_3O_4 , etc.) are chosen to substitute the conventional graphite. Among them, Co_3O_4 has presented excellent characteristics. Firstly, its high theoretical capacity of 890 mAh g^{-1} is ascribed to 8 mol of Li-ion occupying per mole Co_3O_4 [1,2]. Moreover, the methods of synthesizing Co_3O_4 are facile, controllable, and low-cost, by which diverse nanostructured Co_3O_4 materials can be contrived such as nanowires, nanotubes, and nanoparticles. As a consequence, the performance of Co_3O_4 -based anodes can be enhanced by improved surface areas, electrical conductivity, mechanical strength, and Li-ion diffusion efficiency of nanostructured Co_3O_4 . However, the poor conductivity, the massive volumetric expansion of Co_3O_4 during the charge/discharge process, and severe agglomeration trends may cause the pulverization of anode materials and degeneration of the whole electrodes, even serious side reactions [2–4].

Therefore, to address these challenges, researchers often put forward the strategies in the respect of restructuring Co_3O_4 materials and compounding Co_3O_4 with other complementary materials. Commonly, the complementary materials involve carbon nanotube, graphene, and metal materials that feature high electrical conductivity and strong mechanical strength. Prof. Cheng and his research group designed an anode with Co_3O_4 anchored on graphene, which displayed excellent electrochemical performance with superior reversible

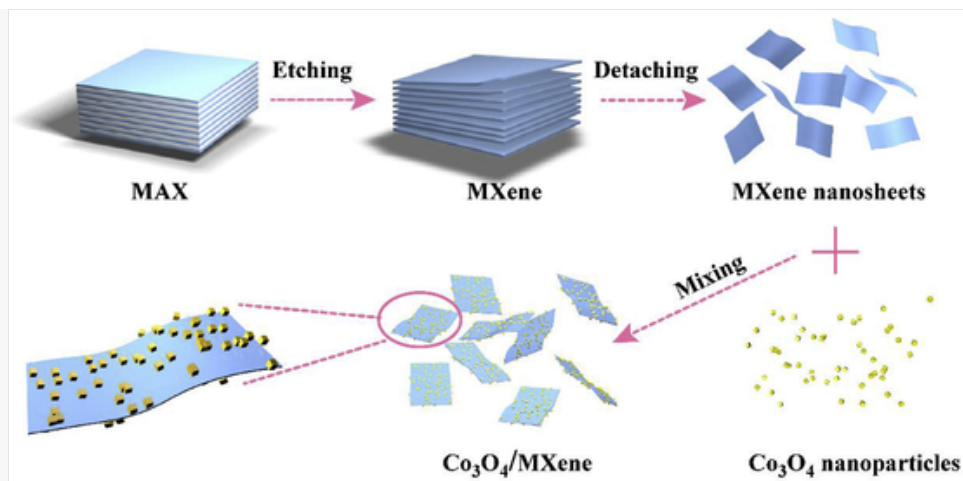
capacity and excellent cycling stability and rate capability [5]. Li and co-workers also synthesized porous Co_3O_4 sheets on graphene foams, which exhibits excellent flexibility and mechanical strength with a high specific capacity of 790 mAh g^{-1} after 100 cycles at a current density of 0.1C [6].

Recently, there is considerable scientific interest in the newly available family of MXenes material. An analog as graphene, this two-dimensional (2D) layered material with the structure of transition metal carbides or nitrides exhibits superior electronic conductivity, large interlayer spacing for highly efficient Li^+ diffusion pathways, and environmental benignity, making it useful as energy storage materials [7]. Gogotsi et al. discovered a novel 2D transition-metal carbide $\text{Ti}_3\text{C}_2\text{T}_x$ (one type of MXene), where T represents the functional groups ($-\text{OH}$, $-\text{F}$, and $-\text{O}$) on the surface. They applied it in transparent and flexible energy storage [8–10]. Their MXene was obtained by removing a group element (IIIA or IVA) layer using HF from the original MAX phases [11], where M is a transition metal, A is an A group of the element, X is C or N. After etching, the MXene was delaminated into few layers leaving large intercalation spacing to enhance Li^+ diffusion. Long-term cycling stability and excellent rate capability were demonstrated by numerous excellent work [12,13]. However, due to their ordinary theoretical capacity of 126.4 mAh g^{-1} at 1 C [14], the challenges remain for their practical applications of energy storage in the near future.

To reveal the importance of introducing MXene as a substitute for graphene in transition metal oxides to promote the electrochemical performance in LIBs, we reported a facile fabrication strategy involving coating the Ni foams with $\text{Co}_3\text{O}_4/\text{MXene}$ mixed suspension layer by layer used as an anode for LIBs (Scheme 1). Four distinguishing features were achieved for this $\text{Co}_3\text{O}_4/\text{MXene}$ composite electrode: (i) The large interlayer spacing of MXene nanosheets allows the Co_3O_4 nanoparticles to distribute uniformly, functioning as a flexible buffer to restrain the volume expansion. (ii) The intercalation of Co_3O_4 in MXene nanosheets prevents not only the agglomeration of Co_3O_4 nanoparticles but also the stacking of MXene nanosheets. (iii) The MXene provides a 3D framework to enhance electrons and Li^+ transmission efficiency. (iv) The mass loading of anode materials on Ni foam increases significantly due to the considerable Co_3O_4 nanoparticles attached to the MXene nanosheets, which offers a large surface area in the nanoscale. Therefore, the $\text{Co}_3\text{O}_4/\text{MXene}$ composite acting as an anode for LIBs delivered 1005 mAh g^{-1} capacity after 300 cycles at the current density of 1 C and remained a stable capacity of 307 mAh g^{-1} at the current density of 5 C after 1000 cycles, displaying outstanding electrochemical performance with superior reversible capacity and excellent cycling stability and rate capability.

alt-text: Scheme 1

Scheme 1



Schematic illustration for the synthesis procedure of Co₃O₄/MXene composite.

2 Experimental section

2.1 Delamination of MXene

To prepare a homogeneous delaminated Ti₃C₂T_x suspension, 2 g Ti₃AlC₂ powders (200 mesh, 11 Technology Co., Ltd) were slowly added to the prepared suspension in which 2 g LiF mixed with 40 mL HCl (9 M) in a Teflon beaker with stirring for 30 min. Then, the above suspension was kept at 35 °C under magnetic stirring for 24 h. The resultant suspension was washed using **deionized (DI) distilled** water accompanied by sonication for 10 min and centrifugation (3500 rpm, 10 min) for many times to remove the residual impurities and HF until the pH of supernatant approaching 6. Moreover, the sediment was dispersed in ethanol that functioned as an intercalation agent and sonicated for 1.5 h followed by centrifugation (10000 rpm, 10 min). Finally, the homogeneous delaminated Ti₃C₂T_x suspension was prepared by repeatedly collecting the supernatant after centrifugation (3500 rpm, 10 min) in which the above sediment was mixed with 20 mL **deionized water (DI)** water under sonication for 20 min.

2.2 Synthesis of Co₃O₄ nanoparticles

The Co₃O₄ nanoparticles were synthesized with reference to Prof. Peng's method [9]. 797 mg Co(CH₃COO)₂·4H₂O (Aladdin Industrial Corporation, China) was dissolved in 16 mL DI **water** followed by stirring, which afterward was slowly dropped into the 160 mL ethanol and stirred for 2 h. The uniform mixture was poured into a 200 mL Teflon-line steel autoclave and heated at 120 °C in a muffle furnace for 8 h. The black precipitate was obtained by centrifugation using ethanol for four times. Eventually, Co₃O₄ nanoparticles were sent into a vacuum oven and kept at 80 °C for 12 h.

2.3 Fabrication of Co₃O₄/MXene composite electrodes

50 mg as-prepared Co₃O₄ nanoparticles were dispersed in 5 mL ethanol under sonication for 20 min. Then, 5 mL MXene suspension (10 mg/mL) was added into the above suspension with stirring for 6 h. The Co₃O₄/MXene composite electrodes were fabricated by dropping the uniform Co₃O₄/MXene suspension onto

the Ni foams (13 mm diameter). In order to obtain the composite electrodes with required mass loading, the above steps were repeated at different times. The composite electrodes were dried in vacuum at 60 °C for 12 h and 120 °C for **another** 3 h. After cooling down to **the** room temperature, these electrodes were sent to the glove box to be assembled into the coin cells. To investigate the effect of different ratios of Co₃O₄ and MXene on the electrochemical performance of LIBs, the ratio was designed, including Co₃O₄/MXene = 1:2, 1:1, 2:1, and 4:1, labeled as COMX0.5, COMX1, COMX2, and COMX4, respectively. The average mass loading of the active material (Co₃O₄) is around 0.8–1 mg cm⁻¹ and the specific data for different composite electrodes is provided in [Table S1](#). Besides, the control groups were obtained by individually dropping the pure Co₃O₄ and pure MXene suspension on the Ni foams.

2.4 Materials characterizations

The crystal structures of Co₃O₄ nanoparticles, MXene nanosheets, and Co₃O₄/MXene composite were investigated by an X-ray diffractometer (XRD, D8 Advance, Bruker) using a Cu K α radiation source from 3° to 80°. Besides, the Raman spectrometer (Jobin YvonXploRA, HORIBA Scientific) was applied to characterize the structure and composition using a 532 nm laser. The microstructure and element distribution of all samples were analyzed by a scanning electron microscope (SEM, Hitachi Regulus 8230) and transmission electron microscopy (TEM, FEI Talos F200x) with energy-dispersive X-ray spectroscopy (EDS).

2.5 Electrochemical measurements

Two-electrode 2032 coin-cells, in which the Co₃O₄/MXene composite electrodes played a role as working electrodes, and the metallic lithium foil acted as both the counter electrode and reference electrodes, were assembled in an argon-filled glove box (Vigor Sci-Lab). Furthermore, the separator (Celgard 2325) and the electrolyte of 1 M LiPF₆ dissolved in a mixture of dimethyl carbonate (DMC) and ethylene carbonate (EC) (1:1 w/w) were employed. Galvanostatic charge-discharge cycling tests were conducted on a battery tester (Neware CT - 4008) with the voltage ranging from 0.01 V to 3.0 V versus Li⁺/Li at various current densities. Both cyclic voltammetry (CV) and electrochemical impedance spectroscopy (EIS) tests were conducted on an Autolab electrochemical workstation (PGSTAT302N). The CV curves were obtained at 0.1 mV s⁻¹ over the same potential range (0.01–3V) while the EIS was tested over a frequency range of 100 kHz to 0.01 Hz with an ac voltage amplitude of 2 mV.

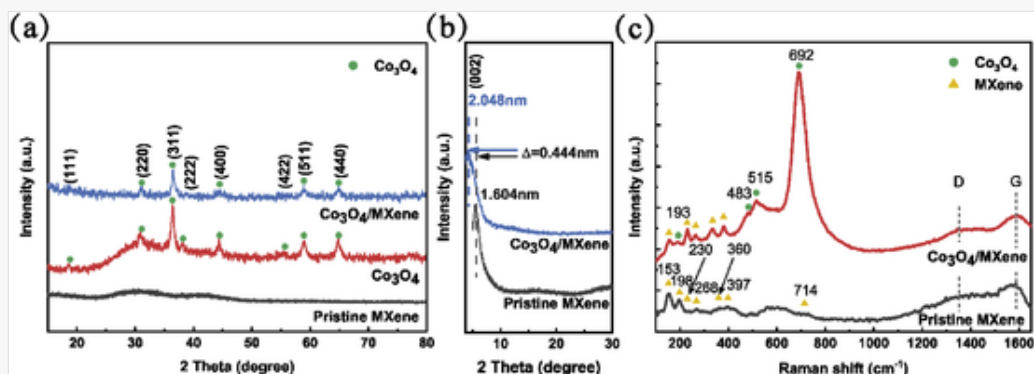
3 Results and discussion

To further illustrate the crystal structure and morphology of the samples, the XRD patterns of Co₃O₄/MXene composite, Co₃O₄ nanoparticles, and MXene nanosheets, are presented in [Fig. 1a](#). The prominent diffraction peaks at 18.9°, 31.2°, 36.8°, 38.5°, 44.9°, 55.6°, 59.5°, and 65.3° are respectively indexed to the (111), (220), (311), (222), (400), (422), (511), and (440) planes of Co₃O₄ nanoparticles (PDF No. 43–1003). A prominent peak at 5.504° is associated with the MXene phase (002), authenticating the successful delamination of MXene nanosheets, as shown in [Fig. 1b](#) [[11,15,16](#)]. The characteristic peaks of both Co₃O₄ and MXene are exhibited in the XRD pattern of Co₃O₄/MXene composite. Interestingly, the central peak (002) of MXene down-shifts to a smaller angle of $2\theta = 4.31^\circ$ indicating the expansion of the MXene nanosheets along the c-axis with the increased interlayer spacing of 2.05 nm according to Bragg's equation [[17–19](#)]. Both the intensity

weakening and down-shift of (002) peak are attributed to the intercalation of Co_3O_4 nanoparticles between the MXene interlayers [11,16]. The resultant larger MXene interlayer spacing is beneficial for not only accommodating the huge volume change of Co_3O_4 nanoparticles but also improving the Li^+ diffusion efficiency with more electrolyte reaching Co_3O_4 nanoparticles.

alt-text: Fig. 1

Fig. 1



(a) XRD patterns of $\text{Co}_3\text{O}_4/\text{MXene}$ composite with the ratio of $\text{Co}_3\text{O}_4/\text{MXene} = 2:1$ (COMX2), Co_3O_4 nanoparticles, and MXene nanosheets. (b) XRD patterns and (c) Raman spectra of COMX2 and MXene nanosheets.

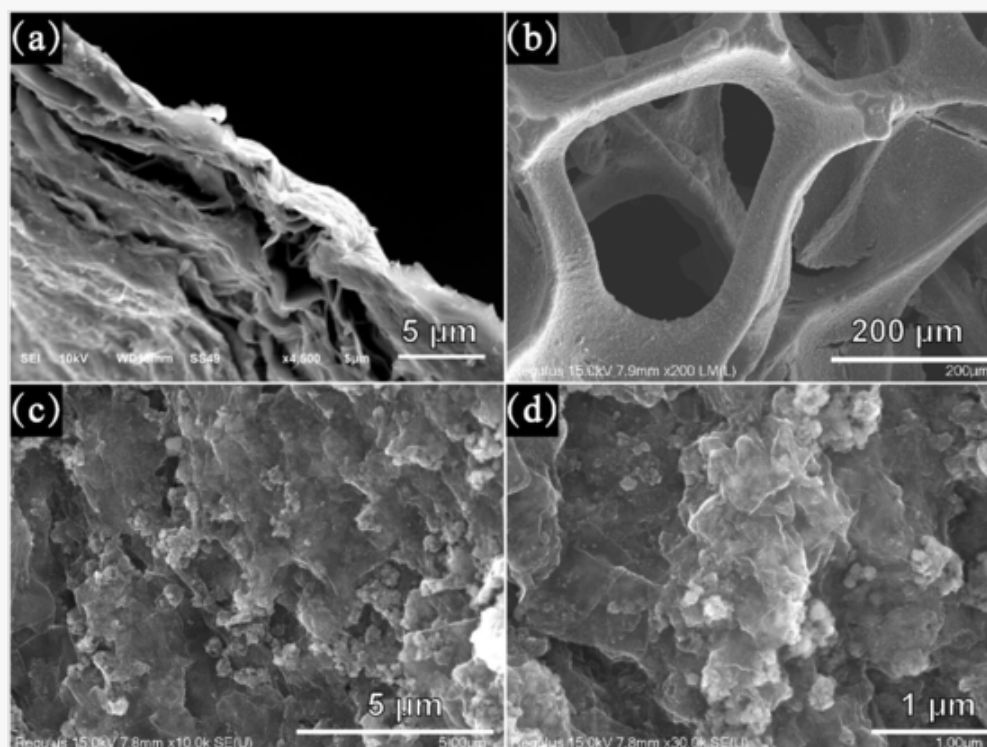
Raman spectra (Fig. 1c) provides additional information about the surface structure of the $\text{Co}_3\text{O}_4/\text{MXene}$ composite. The characteristic bands of both Co_3O_4 nanoparticles and MXene nanosheets were exhibited in the composite. There are two broad peaks around 1350 cm^{-1} (D band) and 1585 cm^{-1} (G band) for graphitic carbon. The I_D/I_G ratio for $\text{Co}_3\text{O}_4/\text{MXene}$ composite about 0.73 is slightly larger than that of pristine MXene nanosheets, implying the attenuated graphitization degree of carbon due to the incorporation of Co_3O_4 nanoparticles [20,21]. Four peaks around 193, 483, 515, and 692 cm^{-1} (labeled with green circles) in the spectrum of the composite are respectively indexed to the F_{2g} , E_g , F_{1g} , and A_{1g} Raman-active modes of the crystalline Co_3O_4 [22–24]. By comparison, the characteristic peaks corresponding to MXene are labeled with yellow triangles. The band at 153 cm^{-1} is related to the Ti-O stretching vibration indicating the oxidation of MXene [25,26]. In addition, the peaks located at 198 and 714 cm^{-1} correspond to A_{1g} symmetry out-of-plane oscillations of Ti and C atoms, while the peaks around 268, 397, and 605 cm^{-1} resulting from the oscillations of E_g group, including in-plane (shear) modes of Ti, C, and surface functional group atoms, [21,27,28].

Fig. 2 shows the morphology of the pure MXene nanosheets and the $\text{Co}_3\text{O}_4/\text{MXene}$ composite on Ni foams. As displayed in Fig. 2a, MXene nanosheets are stacked together with a fluctuant plane, revealing that the flexible MXene could release the strain caused by the volume expansion of Co_3O_4 nanoparticles during the lithiation process. Moreover, the distinct interlayer spacing and the irregular arrangement demonstrate the successful delamination of the MXene nanosheets. The large interlayer spacing is desired to increase the mass loading of active materials and provide more room to accommodate the expansion of active materials. The composite electrode was prepared by coating the $\text{Co}_3\text{O}_4/\text{MXene}$ mixture on the Ni foam, as shown in Fig. 2b. The $\text{Co}_3\text{O}_4/\text{MXene}$ mixture covers the surface of the Ni foam along with the skeleton as well as partially fills

the hole enclosed by the frames, which implies the sufficient contact between the active material with the current collector. In the larger magnification (Fig. 2c and d), Co_3O_4 nanoparticles are distributed within the MXene nanosheets, which can be considered as encapsulated by the MXene nanosheets. In comparison with COMX1, there are more agglomerations for COMX4 due to the higher percentage of the Co_3O_4 nanoparticles leading to the uneven distribution, as displayed in Fig. S1.

alt-text: Fig. 2

Fig. 2



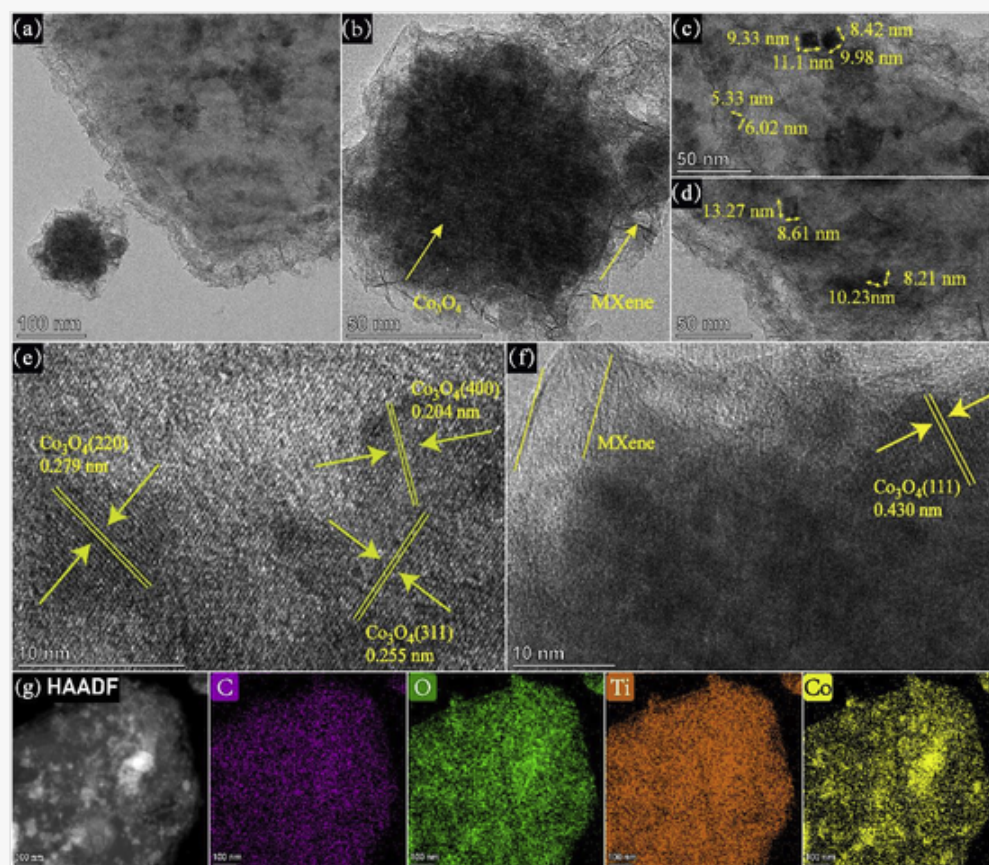
SEM of (a) MXene nanosheets and (b–d) $\text{Co}_3\text{O}_4/\text{MXene}$ composite on Ni foam with the ratio of $\text{Co}_3\text{O}_4/\text{MXene} = 1:1$ (COMX1) with various magnifications.

Fig. 3 displays the TEM images of $\text{Co}_3\text{O}_4/\text{MXene}$ composite with the ratio of $\text{Co}_3\text{O}_4/\text{MXene} = 1:1$ (COMX1). Corresponding to the SEM images, the high-magnification TEM images in Fig. 3a and b also show the Co_3O_4 nanoparticles encapsulated by MXene nanosheets and demonstrate the uniform distribution of Co_3O_4 nanoparticles within the MXene nanosheets. In Fig. 3c and d, the discernible shape of the Co_3O_4 nanoparticles seems to be diamonds with an ultra-small size of 5–15 nm. Co_3O_4 nanoparticles with tiny sizes are beneficial for the efficient diffusion of Li-ion through electrodes and the smaller relative swelling stress created during the lithiation process. In addition, the ultrathin thickness of MXene nanosheets encapsulating the Co_3O_4 nanoparticles approaches 6 nm ~~are approaching transparent in TEM images~~ suggesting the delaminated few-layers of MXene. Meanwhile, these MXene nanosheets are flexible with clearly visible wrinkles on the surface. Observed by the high-resolution TEM (HRTEM), the lattice fringe spacings of different crystals were calculated in Fig. 3e and f. The lattice fringe spacings of 0.430, 0.279, 0.255, and 0.204 nm are assigned to the (111), (220), (311), and (400) planes of Co_3O_4 , respectively, which is consistent

with the characteristic peaks in XRD patterns of $\text{Co}_3\text{O}_4/\text{MXene}$ composite. The EDS element mapping (Fig. 3 g) was conducted to investigate the element distribution in the $\text{Co}_3\text{O}_4/\text{MXene}$ composite. The Co_3O_4 nanoparticles are confirmed by the element O and Co while the element C and Ti demonstrate the existence of MXene nanosheets. It is observed that Co and Ti elements overlap and match well, strongly authenticating a homogeneous distribution of Co_3O_4 nanoparticles within MXene nanosheets. To obtain a high-performance composite electrode, the MXene nanosheets are applied to not only relieve the volume expansion of active materials but also increase the electronic and ionic conductivity of the whole electrode by facilitating the transportation of electrons and reducing the Li^+ diffusion barrier. Hence, the excellent distribution of Co_3O_4 nanoparticles within MXene nanosheets indicates the high-performance of the composite electrode.

alt-text: Fig. 3

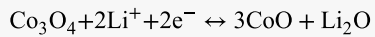
Fig. 3



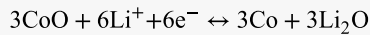
(a–d) High-magnification TEM and (e–f) HRTEM images of $\text{Co}_3\text{O}_4/\text{MXene}$ composite with the ratio of $\text{Co}_3\text{O}_4/\text{MXene} = 1:1$ (COMX1). (g) EDS mapping of the as-obtained COMX1 sample.

To probe the electrochemical performance of the $\text{Co}_3\text{O}_4/\text{MXene}$ composite electrodes, the cyclic voltammetry (CV) was performed at a scan rate of 0.1 mV s^{-1} over a voltage range of 0.01–3 V (vs. Li/Li^+), as shown in Fig. 4a. According to the CV profiles, the lithiation and delithiation processes of Co_3O_4 show a multiple electrochemical reaction behavior [22]. During the first cathodic scan, there is a shoulder peak around 1.4 V corresponding to the reduction procedure from Co_3O_4 to CoO accompanying with the production of Li_2O

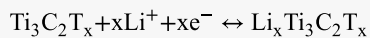
(Equation (1)). After that, a strong and sharp peak appearing at 0.85 V is attributed to the reduction of Co^{2+} to Co^0 and the formation of solid electrolyte interphase (SEI) films (Equation (2)). This reduction peak shifts right to 0.90 V in the following cycles, which indicates not only the irreversible formation of most SEI films but also the activation process of the electrode leading to the more uniform distribution of Co in the Li_2O matrix and higher transmission efficiency of Li-ions [22,28]. Besides, there is a small and broad peak near 0.61 V that is ascribed to the insertion of Li^+ in the MXene nanosheets following Equation (3) [29]. It is more clear to find this reaction peak in the CV curves of the pristine MXene electrode in Fig. S2a. Compared with the pristine MXene electrode, the CV curves of the $\text{Co}_3\text{O}_4/\text{MXene}$ composite electrode exhibit a 10-fold increase in current intensity, which implies that Co_3O_4 nanoparticles dramatically improve the capacitance while the pure MXene is less relevant to the contribution of the capacitance enhancement. During the anodic scan, two distinct peaks are locating at 1.59 and 2.14 V, which are related to the oxidation transformation from metallic Co to Co_3O_4 by two **reversed** steps, respectively. The subsequent CV plots maintain an almost identical shape that reveals the distinguished reversibility of the electrode. After the first cycle, the CVs of the $\text{Co}_3\text{O}_4/\text{MXene}$ composite electrode coincide well to the following cycles, suggesting a good stability and electrochemical reversibility of the composite anode. The corresponding electrochemical reaction equations are shown as follows:



(1)



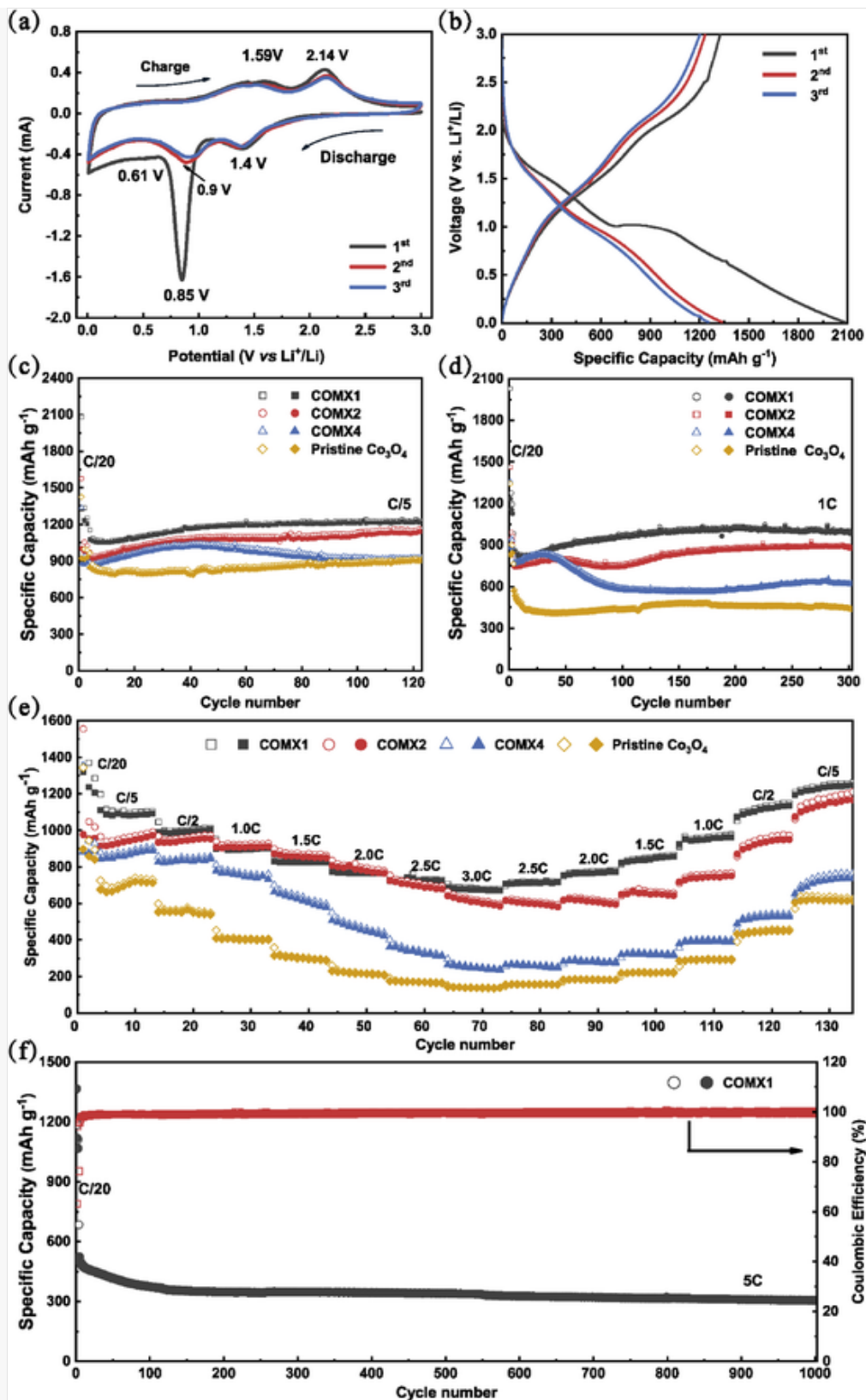
(2)



(3)

alt-text: Fig. 4

Fig. 4



(a) Cyclic voltammetry curves for the initial three cycles for the $\text{Co}_3\text{O}_4/\text{MXene}$ composite electrode (COMX1). (b) Charge/discharge profiles of the COMX1 electrode with the initial three cycles at the current density of C/20 ($C = 890 \text{ mA g}^{-1}$). Cycling performance of $\text{Co}_3\text{O}_4/\text{MXene}$ composite electrode with different ratios of $\text{Co}_3\text{O}_4/\text{MXene} = 1:1, 2:1, \text{ and } 4:1$ (labeled with COMX1, 2, and 4), compared with the pristine Co_3O_4 at the current rates of (c) C/5 and (d) 1 C, respectively. (e) Rate capabilities of COMX electrodes with different ratios and pristine Co_3O_4 electrode. (f) Cycling performance of the COMX1 electrode at the current rate of 5 C.

It is also in good agreement of the galvanostatic charge-discharge (GCD) profiles of the $\text{Co}_3\text{O}_4/\text{MXene}$ composite electrodes for the initial three cycles at $C/20$ in Fig. 4b. In the first discharge profile, two conspicuous discharge plateaus are observed at ~ 1.54 and 1.01 V corresponding to the reduction of Co_3O_4 to metallic Co and the formation of Li_2O , while two broad peaks appearing at $1.57\text{--}1.73$ V and $2.1\text{--}2.3$ V in the first charge profile are associated with the oxidation of the metallic Co accompanying the decomposition of Li_2O to Li. Subsequently, the following cycles exhibit the discharge plateaus with higher voltages, which is consistent with the right shift of the reduction peak in the CV profiles. Moreover, as observed in Fig. 4b, the first discharge capacity approaches 2082 mAh g^{-1} and a charge capacity is around 1326 mAh g^{-1} , which results in an initial coulomb efficiency of $\sim 63.7\%$. On the other hand, the irreversible capacity loss accounts for 36.3% , mainly caused by the formation of SEI films, the irrecoverable conversion of Co_3O_4 , and the partial residual Li^+ in the active materials. Nevertheless, the following cycles exhibit both discharge and charge capacity exceeding the theoretical capacity of 890 mAh g^{-1} . The larger capacity can be ascribed to small contributions from the MXene nanosheets, as shown in Fig. S2b. More importantly, the extra Li-ion storage is attributed to the increased interfacial bonds acting as active sites, which are supplied by the grain boundaries of Li_2O and Co generated during the discharge process [22].

Fig. 4c and d illustrates the cycling performance of the $\text{Co}_3\text{O}_4/\text{MXene}$ composite electrode with different ratios of $\text{Co}_3\text{O}_4/\text{MXene} = 1:1, 2:1, \text{ and } 4:1$ (COMX1, 2, and 4), compared with the pristine Co_3O_4 electrode at the current densities of $C/5$ and $1 C$, respectively. Both tests were conducted with three initial cycles at the rate of $C/20$, aiming to activate and stabilize the batteries. In Fig. 4c, at an initial current density of $C/20$, COMX and pristine Co_3O_4 electrodes show similar initial Coulombic efficiencies between 61 and 65%. With fewer MXene nanosheets involved in the composite, the initial Coulombic efficiencies will increase because of the smaller surface area of the electrode, leading to the less irreversible formation of SEI films. It is further confirmed by the cycling performance of the pristine MXene electrode in Fig. S2b, which shows the first discharge/charge capacities of $186.4/75.5 \text{ mAh g}^{-1}$ resulting in an initial Coulombic efficiency of $\sim 40\%$. The low reversibility of the pristine MXene electrode owes to the considerable functional groups such as $-\text{F}$ and $-\text{OH}$ locating on its surface [24]. Therefore, the lower content of MXene nanosheets in composite results in higher initial Coulombic efficiency. After the three-cycle initialization, COMX1, COMX2, COMX4, and pristine Co_3O_4 electrodes exhibit the reversible capacities of 1155, 973, 886, and 996 mAh g^{-1} , which remains the capacities of 1230, 1167, 932, and 918 mAh g^{-1} after 120 cycles at the rate of $C/5$, with the corresponding retention of 106%, 120%, 105%, and 92%, respectively. It is worth noting that except for the pristine Co_3O_4 electrode, all COMX electrodes increase the capacity by more than 100 percent after 120 cycles, which is caused by the slow activation process for electrolyte ions diffusing through the COMX electrodes when the stacked MXene nanosheets are used [11]. It is further demonstrated in Fig. S2c, where the pristine MXene electrode experiences a minor increase in the specific capacity over a long-term cycling life. Likewise, there are almost identical trends for the cycling performance of COMX and pristine Co_3O_4 electrodes at the rate of $1 C$ in Fig. 4d. Compared with the performance of the pristine Co_3O_4 electrode at $C/5$, the disadvantages of that at $1 C$ become more noticeable, which arises from the low electrical conductivity of the electrode. Among all the COMX electrodes, the COMX1 electrode shows the highest reversible capacity of 1005 mAh g^{-1} after 300 cycles at $1 C$. The higher percentage of MXene nanosheets in the composite leads to the high Li^+ and electrons transmission efficiency between the electrodes. In contrast, the higher content of

Co₃O₄ nanoparticles will not only have a negative effect on the electrical conductivity of the whole electrode but also increase the agglomeration probability of the nanoparticles leading to the uneven distribution Co₃O₄ within the MXene nanosheets. However, if the ratio of Co₃O₄ nanoparticles and MXene nanosheets decreases to a specific value, the cycling performance cannot reach the expectation. For example, the cycling performance of the COMX0.5 electrode (Co₃O₄/MXene = 1:2) was tested at the current density of 1 C in Fig. S3. By contrast, the COMX0.5 electrode delivers a reversible capacity of 678 mAh g⁻¹ after 300 cycles, which is much lower than that of the COMX1 electrode, which is reasonably ascribed to the restacking of MXene nanosheets with fewer Co₃O₄ nanoparticles as spacers. Indeed, Co₃O₄ nanoparticles play a critical role in separating the MXene nanosheets to prevent them from restacking. Hence, the synergistic effect of MXene nanosheets and Co₃O₄ nanoparticles in the COMX1 electrode fulfills its utmost efficiency.

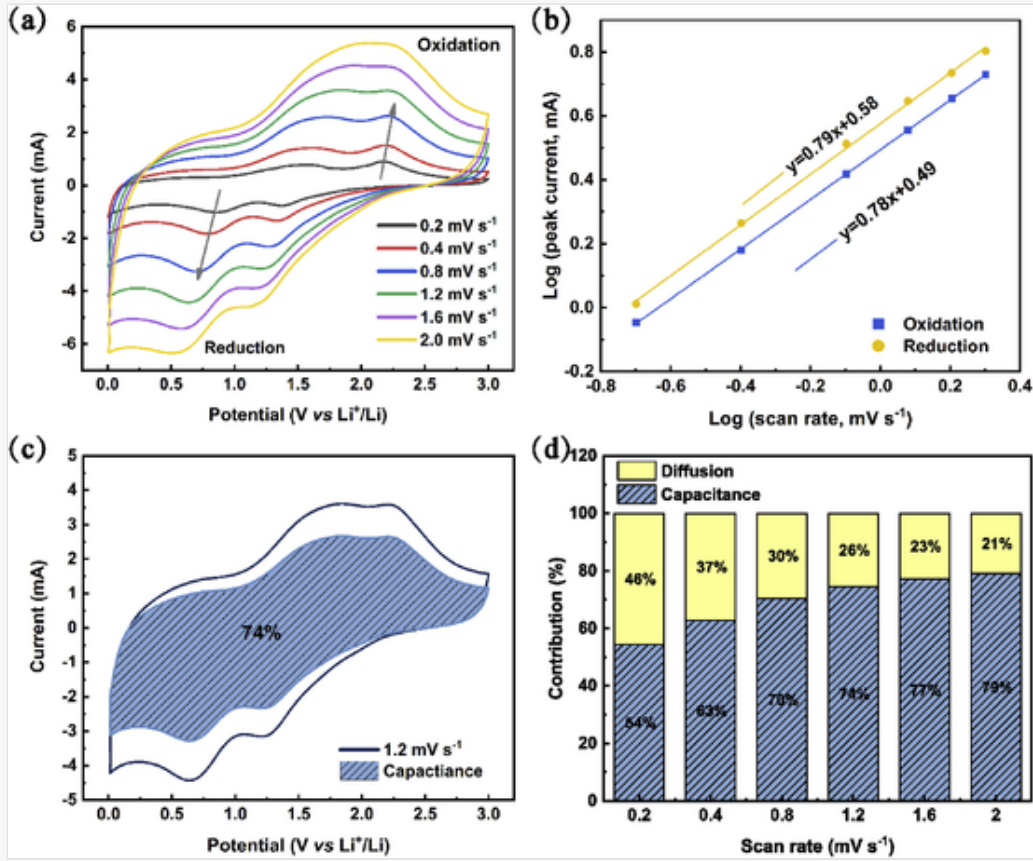
Excellent rate performance of electrode demonstrates the capability of electrodes to support the fast charge and discharge. Fig. 4e shows the rate capability of the COMX and pristine Co₃O₄ electrodes at various current densities of C/5, C/2, 1 C, 1.5C, 2 C, 2.5C, to 3 C and then back at same rates. The COMX1 electrode delivers the capacities retentions of 100%, 87%, 82%, 75%, 72%, 65%, and 64%, at the current densities from C/5 to 3 C, respectively. When the current densities return from 3 C to C/5, there is a little increase in the cycling performance due to the laggardly activated Li-ion transporting through the electrodes. Additionally, the COMX1 electrode remains the highest reversible capacities among all electrodes, which are further demonstrated in the Nyquist plots in Fig. S4. The addition of MXene nanosheets can effectively reduce the charge-transfer impedance of Co₃O₄-nanoparticles the composite electrode, which is consistent with the reduced diameter of the semicircle at the high-frequency region. Accordingly, the COMX1 has the smallest impedance around 35 Ω. Interestingly, when the current density increases to 5 C as illustrated in Fig. 4f, the COMX1 electrode can show a discharge capacity of 307 mAh g⁻¹ after 1000 cycles, which implies the long-term stability of the COMX1 electrode. Similarly, the pristine MXene electrode remains the capacity of 76% after 1000 cycles (Fig. S2c). Therefore, the incorporation of MXene nanosheets with Co₃O₄ enhances the electrical conductivity of the electrode as well as stabilizes the electrode over the long-term cycling by relieving the stress arising from the expansion of active materials.

Typically, the capacity of the Co₃O₄/MXene composite electrode is mainly contributed by diffusion-controlled capacity from conversion and alloying reactions and capacitive capacity caused by surface charge transfer [30]. To further understand the electrochemical kinetics of the COMX1 electrode for Li-ion storage, the corresponding CV curves at scan rates ranging from 0.2 to 2 mV s⁻¹ were carried out, as shown in Fig. 5a. The relationship between the current (i) on scan rate (v) can be expressed with Equations (4) and (5) [28].

$$i = av^b \quad (4)$$

$$\log(i) = b \log(v) + \log(a) \quad (5)$$

Fig. 5



(a) CV curves of COMX1 electrode at different sweep speeds of 0.2, 0.4, 0.8, 1.2, 1.6, and 2.0 mV s⁻¹. (b) Plots of $\log(i)$ versus $\log(v)$ depending on reduction and oxidation peaks. (c) Separated diffusion and capacitive current at a scan rate of 1.2 mV s⁻¹. (d) The ratios of the diffusion and capacitive-controlled contributions at different scan rates.

Both a and b are tunable parameters, whose value could be determined by the intercept and slope of the plot ($\log(i)$ versus $\log(v)$), as illustrated in Fig. 5b. Generally, $b = 0.5$ represents an ideal diffusion-controlled intercalation procedure and $b = 1$ indicates the surface-induced capacitive procedure. According to Fig. 5b, b is equal to 0.79 and 0.78 for oxidation and reduction, respectively, implying the concurrence of two kinds of capacity contributions in the COMX1 electrode. Moreover, the proportion of two-kind contributions can be quantitatively confirmed by separating the current response (i) at a fixed potential V into the capacitive process (k_1v) and the diffusion-controlled process ($k_2v^{0.5}$) following Equation (6) [24,31].

$$i(V) = k_1v + k_2v^{0.5} \quad (6)$$

To determine the constant value of k_1 and k_2 , Equation (6) was transformed into Equation (7) by dividing the $v^{0.5}$ at both sides [32]. Hence, k_1 and k_2 are determined by the slope and intercept of the plots of $i(V)/v^{0.5}$ and

$v^{0.5}$.

$$i(V)/v^{0.5} = k_1 v^{0.5} + k_2$$

(7)

With the explicit k_1 and k_2 , the contribution from the capacitive process ($k_1 v$) and the diffusion-controlled process ($k_2 v^{0.5}$) were calculated. For example, the typical voltage profile at the scan rate of 1.2 mV s^{-1} was shown in Fig. 5c, in which a dominating capacitive current (shadow region) accounts for $\sim 74\%$ compared with the total current, revealing that the electrode is inclined to surface-induced charge storage procedure. With the increasing sweep rate, the COMX1 electrode displays enlarged capacitive contributions of 54%, 63%, 70%, 74%, 77%, and 79%, respectively (Fig. 5d). Interestingly, it is the surface-induced capacitive procedure that plays a significant role in the total current, which is ascribed to the tiny-size Co_3O_4 nanoparticles and stable composite structure. Moreover, the highly conductive MXene nanosheets favor the charge transfer kinetics in the composite electrode. Therefore, the dominating surface-induced capacitive procedure contributes to enhancing the rate capability of the COMX1 electrode, which also explains that the COMX1 electrode delivers a much larger capacity than the theoretical capacity.

4 Conclusion

In conclusion, the $\text{Co}_3\text{O}_4/\text{MXene}$ composite electrodes can be prepared with high performance for the enhanced lithium-ion batteries. The highly conductive MXene nanosheets not only serve as substrates for Co_3O_4 nanoparticles to relieve the stress, but also promote the electronic and ionic conductivity of the whole electrode. Moreover, the synergistic effect of MXene and Co_3O_4 results in excellent stability and electrochemical reversibility. In particular, for the ratios studied here the $\text{Co}_3\text{O}_4/\text{MXene}$ composite electrode with the ratio of $\text{Co}_3\text{O}_4/\text{MXene} = 1:1$ delivered a superb reversible capacity of 1005 mAh g^{-1} after 300 cycles at the current density of 1 C and remained a high capacity of 307 mAh g^{-1} after 1000 cycles at a larger current density of 5 C. The facile preparation method and the excellent electrochemical performance of $\text{Co}_3\text{O}_4/\text{MXene}$ composite electrodes promise it as a competitive anode for lithium-ion batteries.

CRedit authorship contribution statement

Yinchao Zhao: Conceptualization, Methodology, Investigation, Writing - original draft, Writing - review & editing. **Chenguang Liu:** Conceptualization, Methodology, Writing - review & editing. **Ruwei Yi:** Conceptualization, Writing - review & editing. **Ziqian Li:** Methodology, Investigation. **Yanbing Chen:** Methodology, Investigation. **Yinqing Li:** Resources. **Ivona Mitrovic:** Supervision. **Stephen Taylor:** Supervision. **Paul Chalker:** Supervision. **Li Yang:** Resources, Writing - original draft, Writing - review & editing, Supervision, Funding acquisition. **Cezhou Zhao:** Resources, Supervision, Funding acquisition.

Declaration of competing interest

The authors declare that they have no known competing financial interests or personal relationships that could have appeared to influence the work reported in this paper.


Acknowledgments

This work was supported by the National Natural Science Foundation of China (NSFC Grants 21750110441), State Key Laboratory of Materials Processing and Die & Mould Technology, Huazhong University of Science and Technology (P2019-019), Suzhou Industrial Park Initiative Platform Development for Suzhou Municipal Key Lab for New Energy Technology (RR0140), and Key Program Special Fund in XJTLU (KSF-A-04, KSF-E-28).

Appendix A Supplementary data

Supplementary data to this article can be found online at <https://doi.org/10.1016/j.electacta.2020.136203>.

References

 The corrections made in this section will be reviewed and approved by a journal production editor. The newly added/removed references and its citations will be reordered and rearranged by the production team.

- [1] Wang L., Yuan Y.F., Chen Q., Zheng Y.Q., Yin S.M., Guo S.Y., Construction of Co_3O_4 three-dimensional mesoporous framework structures from zeolitic imidazolate framework-67 with enhanced lithium storage properties, *Nanotechnology* 30 (2019) 435402.
- [2] Fan L., Zhang W., Zhu S., Lu Y., Enhanced lithium storage capability in Li-ion batteries using porous 3D Co_3O_4 nanofiber anodes, *Ind. Eng. Chem. Res.* 56 (2017) 2046–2053.
- [3] Lee C., Park Y., Carbon and binder-free air electrodes composed of Co_3O_4 nanofibers for Li-air batteries with enhanced cyclic performance, *Nanoscale Research Letters* 10 (2015) 1027.
- [4] Chen J., Xia X.h., Tu J.p., Xiong Q.q., Yu Y.X., Wang X.l., Gu C.d., Co_3O_4 –C core–shell nanowire array as an advanced anode material for lithium ion batteries, *J. Mater. Chem.* 22 (2012) 15056.
- [5] Wu ZhongShuai, Ren Wencai, Wen Lei, Gao Libo, Zhao Jinping, Chen Zongping, Zhou Guangmin, Li Feng, Cheng a.H.M., Graphene anchored with Co_3O_4 nanoparticles as anode of lithium ion batteries with enhanced reversible capacity and cyclic performance, *ACS Nano* 4 (2010) 3187–3194.
- [6] Yao Y., Zhu Y., Zhao S., Shen J., Yang X., Li C., Halide ion intercalated electrodeposition synthesis of Co_3O_4 nanosheets with tunable pores on graphene foams as free-standing and flexible Li-ion battery anodes, *ACS Appl. Energy Mater.* 1 (2018) 1239–1251.
- [7] Luo J., Tao X., Zhang J., Xia Y., Huang H., Zhang L., Gan Y., Liang C., Zhang W., Sn^{4+} ion decorated highly conductive Ti_3C_2 MXene: promising lithium-ion anodes with enhanced volumetric capacity and cyclic performance, *ACS Nano* 10 (2016) 2491–2499.

- [8] Zhang Y., Mu Z., Lai J., Chao Y., Yang Y., Zhou P., Li Y., Yang W., Xia Z., Guo S., MXene/Si@SiOx@C layer-by-layer superstructure with autoadjustable function for superior stable lithium storage, *ACS Nano* 13 (2019) 2167–2175.
- [9] Luo S., Wang R., Yin J., Jiao T., Chen K., Zou G., Zhang L., Zhou J., Zhang L., Peng Q., Preparation and dye degradation performances of self-assembled MXene-Co₃O₄ nanocomposites synthesized via solvothermal approach, *ACS Omega* 4 (2019) 3946–3953.
- [10] Sun S., Liao C., Hafez A.M., Zhu H., Wu S., Two-dimensional MXenes for energy storage, *Chem. Eng. J.* 338 (2018) 27–45.
- [11] Zhao M.Q., Torelli M., Ren C.E., Ghidui M., Ling Z., Anasori B., Barsoum M.W., Gogotsi Y., 2D titanium carbide and transition metal oxides hybrid electrodes for Li-ion storage, *Nanomater. Energy* 30 (2016) 603–613.
- [12] Mashtalir O., Naguib M., Mochalin V.N., Dall’Agnese Y., Heon M., Barsoum M.W., Gogotsi Y., Intercalation and delamination of layered carbides and carbonitrides, *Nat. Commun.* 4 (2013) 1716.
- [13] Sun D., Wang M., Li Z., Fan G., Fan L.-Z., Zhou A., Two-dimensional Ti₃C₂ as anode material for Li-ion batteries, *Electrochem. Commun.* 47 (2014) 80–83.
- [14] Kong F., He X., Liu Q., Qi X., Zheng Y., Wang R., Bai Y., Improving the electrochemical properties of MXene Ti₃C₂ multilayer for Li-ion batteries by vacuum calcination, *Electrochim. Acta* 265 (2018) 140–150.
- [15] Tian Y., An Y., Feng J., Flexible and freestanding silicon/MXene composite papers for high-performance lithium-ion batteries, *ACS Appl. Mater. Interfaces* 11 (2019) 10004–10011.
- [16] Deng R., Chen B., Li H., Zhang K., Zhang T., Yu Y., Song L., MXene/Co₃O₄ composite material: stable synthesis and its enhanced broadband microwave absorption, *Appl. Surf. Sci.* 488 (2019) 921–930.
- [17] Zhang P., Zhu Q., Guan Z., Zhao Q., Sun N., Xu B., A flexible Si@C electrode with excellent stability employing an MXene as a Multifunctional Binder for Lithium-Ion Batteries 13 (2020) 1621–1628.
- [18] Liu Y.T., Zhang P., Sun N., Anasori B., Zhu Q.Z., Liu H., Gogotsi Y., Xu B., Self-assembly of transition metal oxide nanostructures on MXene nanosheets for fast and stable lithium storage, *Adv. Mater.* 30 (2018) 1707334.
- [19] Lukatskaya M.R., Mashtalir O., Ren C.E., Dall’Agnese Y., Rozier P., Taberna P.L., Naguib M., Simon P., Barsoum M.W., Gogotsi Y., Cation intercalation and high volumetric capacitance of two-dimensional titanium carbide, *Science* 341 (2013) 1502–1505.

[20]

Ma Z., Zhou X., Deng W., Lei D., Liu Z., 3D porous MXene (Ti_3C_2)/reduced graphene oxide hybrid films for advanced lithium storage, *ACS Appl. Mater. Interfaces* 10 (2018) 3634–3643.

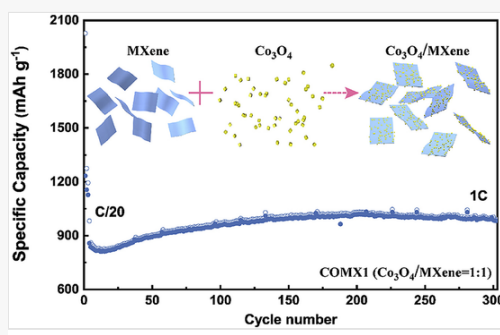
- [21] Yan J., Ren C.E., Maleski K., Hatter C.B., Anasori B., Urbankowski P., Sarycheva A., Gogotsi Y., Flexible MXene/graphene films for ultrafast supercapacitors with outstanding, Volumetric Capacitance 27 (2017) 1701264.
- [22] Liu M., Deng X., Ma Y., Xie W., Hou X., Fu Y., He D., Well-designed hierarchical Co_3O_4 architecture as a long-life and ultrahigh rate capacity anode for advanced lithium-ion batteries, *Advanced Materials Interfaces* 4 (2017) 1700553.
- [23] Chen Y., Wang Y., Wang Z., Zou M., Zhang H., Zhao W., Yousaf M., Yang L., Cao A., Han R.P.S., Densification by compaction as an effective low-cost method to attain a high areal lithium storage capacity in a $\text{CNT}@\text{Co}_3\text{O}_4$, *Sponge* 8 (2018) 1702981.
- [24] Sun X., Tan K., Liu Y., Zhang J., Denis D.K., Zaman F.U., Hou L., Yuan C., A two-dimensional assembly of ultrafine cobalt oxide nanocrystallites anchored on single-layer $\text{Ti}_3\text{C}_2\text{T}_x$ nanosheets with enhanced lithium storage for Li-ion batteries, *Nanoscale* 11 (2019) 16755–16766.
- [25] Zuo D.C., Song S.C., An C.s., Tang L.B., He Z.J., Zheng J.C., Synthesis of sandwich-like structured $\text{Sn}/\text{SnOx}@\text{MXene}$ composite through in-situ growth for highly reversible lithium storage, *Nanomater. Energy* 62 (2019) 401–409.
- [26] Deng Y., Shang T., Wu Z., Tao Y., Luo C., Liang J., Han D., Lyu R., Qi C., Lv W., Kang F., Yang Q.H., Fast gelation of $\text{Ti}_3\text{C}_2\text{T}_x$ MXene initiated by metal ions, *Adv. Mater.* (2019) 1902432.
- [27] Naguib M., Mashtalir O., Lukatskaya M.R., Dyatkin B., Zhang C., Presser V., Gogotsi Y., Barsoum M.W., One-step synthesis of nanocrystalline transition metal oxides on thin sheets of disordered graphitic carbon by oxidation of MXenes, *Chem. Commun.* 50 (2014) 7420–7423.
- [28] Zhao X., Xu H., Hui Z., Sun Y., Yu C., Xue J., Zhou R., Wang L., Dai H., Zhao Y., Yang J., Zhou J., Chen Q., Sun G., Huang W., Electrostatically assembling 2D nanosheets of MXene and MOF-derivatives into 3D hollow frameworks for enhanced lithium storage, *Small* (2019) 1904255.
- [29] Yang C., Liu Y., Sun X., Zhang Y., Hou L., Zhang Q., Yuan C., In-situ construction of hierarchical accordion-like $\text{TiO}_2/\text{Ti}_3\text{C}_2$ nanohybrid as anode material for lithium and sodium ion batteries, *Electrochim. Acta* 271 (2018) 165–172.
- [30] Li Q., Zhao Y., Liu H., Xu P., Yang L., Pei K., Zeng Q., Feng Y., Wang P., Che R., Dandelion-Like Mn/Ni Co-doped CoO/C hollow microspheres with oxygen vacancies for advanced lithium storage, *ACS Nano* 13 (2019) 11921–11934.
- [31] Brezesinski T., Wang J., Polleux J., Dunn B., Tolbert S.H., Templated nanocrystal-based porous TiO_2 films for next-generation electrochemical capacitors, *J. Am. Chem. Soc.* 131 (2009) 1802–1809.

[32] Chao D., Zhu C., Yang P., Xia X., Liu J., Wang J., Fan X., Savilov S.V., Lin J., Fan H.J., Shen Z.X., Array of nanosheets render ultrafast and high-capacity Na-ion storage by tunable pseudocapacitance, Nat. Commun. 7 (2016) 12122.

Graphical abstract

The scheme illustrates a facile strategy of mixing MXene nanosheets and Co_3O_4 NPs to form the $\text{Co}_3\text{O}_4/\text{MXene}$ composite. The composite electrode with the mass ratio of $\text{Co}_3\text{O}_4/\text{MXene} = 1:1$ fabricated by this strategy delivers an excellent capacity of $1005 \text{ mA}\cdot\text{g}^{-1}$ after 300 cycles at the current densities of 1 C ($C = 890 \text{ mA}\cdot\text{g}^{-1}$).

alt-text: Image 1



Highlights

- Co_3O_4 nanoparticles/MXene nanosheets composite was prepared on the nickel foams.
- MXene nanosheets acted as a buffer to accommodate the volume change of active materials as well as prevent the agglomeration of Co_3O_4 nanoparticles.
- MXene nanosheets were used to improve the conductivity of the electrode.

Appendix A Supplementary data

The following is the Supplementary data to this article:

[Multimedia Component 1](#)

Multimedia component 1

Queries and Answers

Query: Your article is registered as a regular item and is being processed for inclusion in a regular issue of the journal. If this is NOT correct and your article belongs to a Special Issue/Collection please contact a.elumalai@elsevier.com immediately prior to returning your corrections.

Answer: Yes

Query: Please confirm that given names and surnames have been identified correctly and are presented in the desired order and please carefully verify the spelling of all authors' names.

Answer: Yes

Query: Please confirm that the provided emails “cezhou.zhao@xjtlu.edu.cn, li.yang@xjtlu.edu.cn” are the correct address for official communication, else provide an alternate e-mail address to replace the existing one, because private e-mail addresses should not be used in articles as the address for communication.

Answer: yes, they are correct address for official communication.

Query: For figure(s) 1, All supplied figures are followed by Manuscript-revised.docx format.kindly check carefully and confirm accuracy.

Answer: Yes, I have checked it.

Query: Have we correctly interpreted the following funding source(s) and country names you cited in your article: National Natural Science Foundation of China, China; Huazhong University of Science and Technology, China?

Answer: Yes

Query: Highlights should only consist of “125” characters per bullet point, including spaces. The highlights provided are too long; please edit them to meet the requirement.

Answer: I have changed the highlights.